RSC Advances

PAPER

View Article Online
View Journal | View Issue

Open Access Article. Published on 03 March 2026. Downloaded on 3/16/2026 10:14:35 PM.
This article is licensed under a Creative Commons Attribution-NonCommercial 3.0 Unported Licence.

Check for updates

Cite this: *RSC Adv.*, 2026, **16**, 12180

2-Pyridone-assisted palladium-catalyzed regioselective arylation of naphthamides

Jayprakash Prajapati and Sourav Chatterjee *

Received 14th January 2026
Accepted 12th February 2026

DOI: 10.1039/d6ra00358c

rsc.li/rsc-advances

The 2-pyridone scaffold receives attention in medicinal chemistry due to its bioisostere properties, which significantly contributing to lipophilicity, solubility, metabolic stability, and drug off-target effects. In the present article, we report the 2-pyridone-assisted regioselective arylation of naphthamides. Using diversified naphthamides and aryl iodides, a wide variety of 2-pyridone-containing molecular scaffolds were synthesized in good yields, which could be potentially useful in medicinal chemistry.

Introduction

The development of a new potential drug molecule has always been associated with many challenges. Design of a molecular architecture and its compelling synthetic approach for a specific biological function always remain a challenge. The 2-pyridone scaffold functions both as a hydrogen-bond acceptor and donor; serves as a bioisostere for amides, phenyls, pyridines, and other N- or O-containing heterocycles; and modulates lipophilicity, aqueous solubility, and metabolic stability in drug molecules. Compared to phenyls, pyridines, or phenols, pyridones are more polar (higher $c\log P$, $\log D$, and PSA values), often resulting in improved drug-like properties. Unlike basic nitrogen heterocycles, such as pyridine, the neutral, less lipophilic pyridone ring system helps reduce off-target activities. Its embedded amide functionality makes 2-pyridone a valid peptide-bond isostere and improves its physicochemical properties, such as metabolic clearance. Fig. 1 highlights a few representative examples of how the systematic incorporation of 2-pyridone onto a hit molecule through structure–activity relationship (SAR) studies could afford an optimized lead molecule with improved potency.[1–5] Similarly, Kohji Hanasaki and co-workers developed a human cannabinoid receptor type II (CB2R) inhibitor bearing the 2-pyridone backbone that regulates analgesic and anti-inflammatory responses without central adverse effects.[6] Stephen T. Worland and co-workers report 2-pyridone-containing HRV-2 3CP inhibitors as anti-rhinoviral agents.[7] Another report from Alan S. Rosenthal and co-workers highlights HLE inhibitors bearing the 2-pyridone moiety, used for the treatment of emphysema and cystic fibrosis.[8]

Owing to the growing application of 2-pyridone as a fundamental heterocyclic building block in medicinal chemistry, we planned to explore its use as a directing group for facile access to important molecular architectures, which potentially could be used in medicinal chemistry. As a proof of concept, initially, we chose the naphthamide system for 2-pyridone-mediated regioselective sp^2 C–H activation.

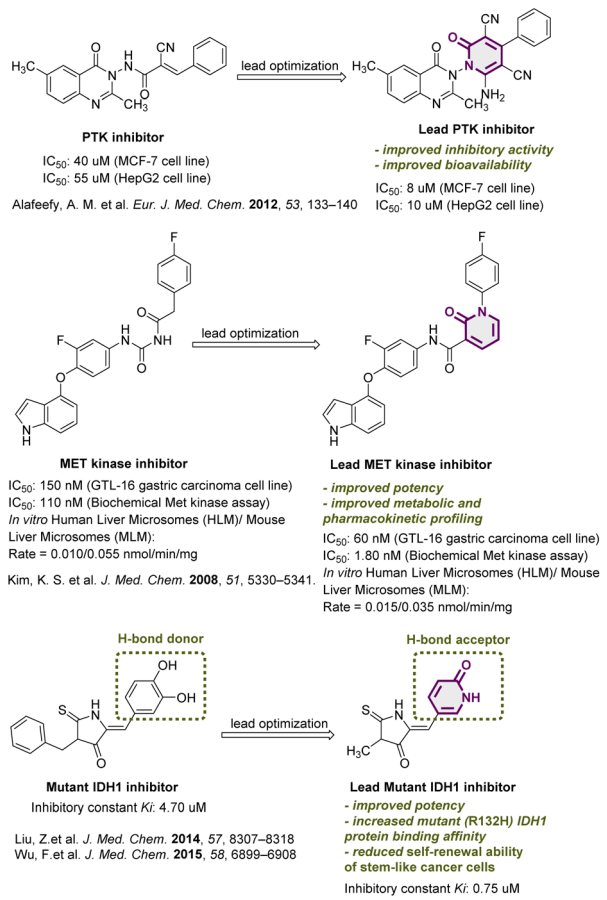

Fig. 1 2-Pyridone molecular scaffold in optimized-lead-molecule identification.

Department of Chemistry, Ashoka University, Sonipat, Haryana-131029, India. E-mail: sourav.chatterjee@ashoka.edu.in

© 2026 The Author(s). Published by the Royal Society of Chemistry

Open Access Article. Published on 03 March 2026. Downloaded on 3/16/2026 10:14:35 PM.
This article is licensed under a Creative Commons Attribution-NonCommercial 3.0 Unported Licence.

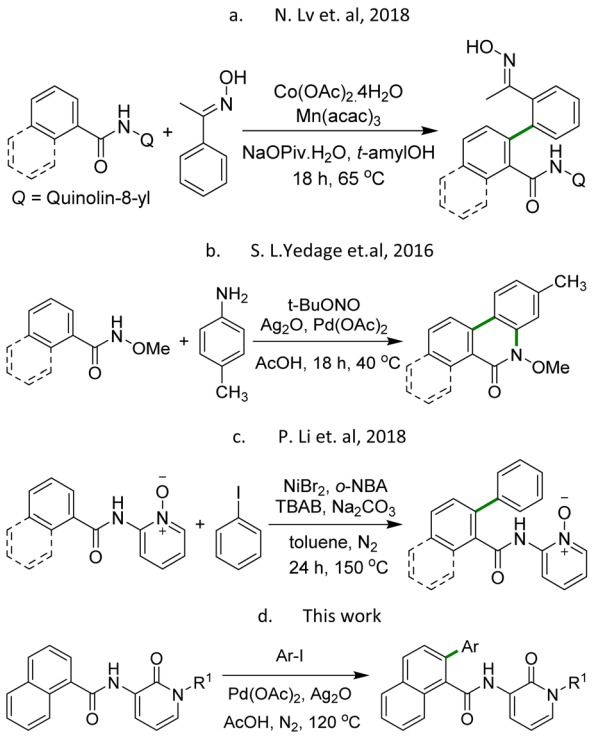

Scheme 1 Regioselective C2–H arylation of 1-naphthamides.

Regioselective C–H activation in naphthamide is important because it allows late-stage functionalization of complex naphthalene-containing molecules, useful in drug molecules, fungicides, organic electronics, dyes and pigments. In 2018, N. Lv *et al.* showcased Co and Mn-dual catalysis cross-coupling as a strategy for chelation-assisted C–H activation from readily available benzamides and oximes (Scheme 1a). The resulting difunctional biaryl synthesis also responded well for 1-naphthamide (Scheme 1a).[9] This dual-chelation-assisted strategy provides access to diverse difunctional biaryls, which offer promising biological activities considering their substrate scope and controlled regioselectivity. B. M. Bhanage and coworkers in 2016 implemented a deaminative C–C bond coupling using *N*-methoxybenzamide/naphthamide in combination with aromatic amines and $Pd(OAc)_2$ as a catalyst to generate diverse phenanthridinones (Scheme 1b).[10] Along this line, a report by P. Li *et al.* in 2018 disclosed the nickel-catalyzed regioselective arylation of aromatic amides with aryl iodides, where pyridine-*N*-oxide served as a directing group (Scheme 1c).[11]

Owing to the importance of 2-pyridone in medicinal chemistry and its growing functional utility as a directing group,[12] here, we report 2-pyridone as a bidentate directing group for the regioselective sp^2 C–H arylation of 1-naphthamide. To the best of our knowledge, this is the first study to adopt 2-pyridone as a directing group for the regioselective C2 arylation of 1-naphthamide. This 2-pyridone-assisted C2–H arylation proceeds *via* Pd catalysis (with Ag_2O employed for catalyst regeneration) in acetic acid as a solvent, affording *N*-(1-alkyl-2-pyridone-3-yl)-2-aryl-1-naphthamides in good-to-excellent yields (Scheme 1d).

Results and discussion

To optimize the 2-pyridone-directed regioselective C2–H arylation of 1-naphthamide, we first considered *N*-(1-methyl-2-pyridone)-2-phenyl-1-naphthamide (**4a1**) as a representative example to start with. The precursor *N*-(1-methyl-2-pyridone)-1-naphthamide (**3a**) was synthesized from the *N*-methylation of 3-nitro-2-pyridone (**1a**), followed by the reduction of its nitro group to amine (**2a**) and, further, its conjugation with 1-naphthoic acid *via* acid-amine coupling to form the corresponding *N*-(1-methyl-2-pyridone-3-yl)-1-naphthamide (**3a**) (Scheme 2). We tested our hypothesis with 10 mol% $Pd(OAc)_2$ and 0.36 mmol (2 eqv.) Ag_2O under inert conditions, at 80 °C for 10 h (Table 1, entry 1). Further isolation and characterization confirmed the formation of **4a1** as the desired product in 25% isolated yield (Table 1, entry 1). To optimize the reaction condition, we planned to determine the yield of the crude reaction mixture by HPLC analysis. A growth curve was generated using HPLC for **4a1**, with an increase in the **4a1** product concentration. The reaction temperature was further increased to 100 °C, 120 °C and then to 150 °C. An increase in the yield was observed when the reaction temperature was raised to 100 °C (73%) and 120 °C (96%) (Table 1, entry 2–3). However, further increase in the reaction temperature to 150 °C reduced the yield to 71% (Table 1, entry 4), which could be because trace impurity formation was observed at this temperature. Under this condition, reducing the reaction time to 6 h or increasing the reaction time to 15 h had a very little influence in terms of product yield (Table 1, entries 5–6). We further extended our observation to determine the right solvent for this reaction. While H_2O and HFIP offered negligible and moderate reaction yields (Table 1, entries 7 and 8), respectively, using an identical acetic-acid composition (1 : 1) with these solvents did not greatly enhance the reaction outcome (Table 1, entries 9–10). The use of DMF also failed to establish it as a solvent of choice (Table 1, entry 11). Our findings highlight acetic acid as the optimized solvent tested. We were curious to understand the effect of other additives compared to Ag_2O. Ag_2CO_3 (2.0 eqv., 0.36 mmol) and

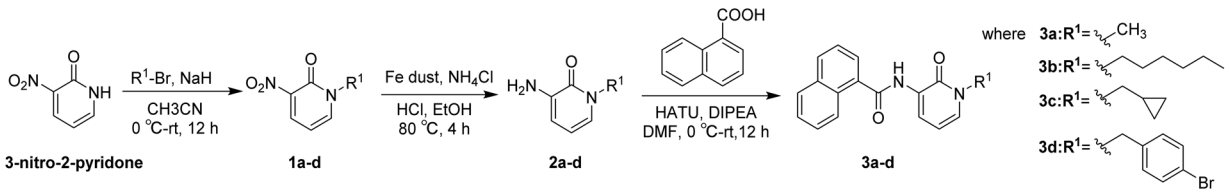

Scheme 2 Synthetic route for the *N*-(1-alkyl-2-pyridone-3-yl)-1-naphthamides.

Open Access Article. Published on 03 March 2026. Downloaded on 3/16/2026 10:14:35 PM.
This article is licensed under a Creative Commons Attribution-NonCommercial 3.0 Unported Licence.

Table 1 Optimization of the reaction conditions[a]

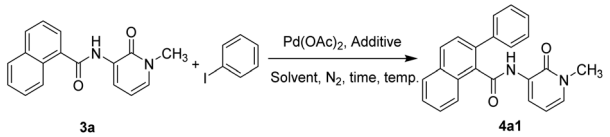

Entry	Additive/Temp. (°C)/Time (h)	Solvent	Yield[g] (%)
1	Ag_2O/80/10	AcOH	32 (25[i])
2	Ag_2O/100/10	AcOH	73
3	**Ag_2O/120/10**	**AcOH**	**96 (86[i])**
4	Ag_2O/150/10	AcOH	71
5	Ag_2O/120/6	AcOH	87
6	Ag_2O/120/15	AcOH	89
7	Ag_2O/120/10	H_2O	6
8	Ag_2O/120/10	HFIP	65
9	Ag_2O/120/10	H_2O : AcOH (1 : 1)	24
10	Ag_2O/120/10	HFIP : AcOH (1 : 1)	69
11	Ag_2O/120/10	DMF	Trace
12[b]	Ag(OAc)/CF_3COONa/120/10	AcOH	45
13[b]	Ag(OAc)/CF_3COONa/120/10	Dioxane	67
14[c]	Ag_2O/120/10	AcOH	91
15[d]	Ag_2O/120/10	AcOH	88
16[e]	Ag_2O/120/10	AcOH	48
17[f]	Ag_2O/120/10	AcOH	41
18[h]	Ag_2CO_3/120/10	AcOH	91[i]

[a] Reaction conditions: **3a** (0.18 mmol), Ph-I (0.36 mmol), $Pd(OAc)_2$ (10 mol%), and Ag_2O (0.36 mmol), heated at a specified temperature for the mentioned time. [b] 0.54 mmol of Ag(OAc) and 0.36 mmol of CF_3COONa were used. [c] Ag_2O (0.27 mmol). [d] Ag_2O (0.18 mmol). [e] $Pd(Oac)_2$ (5 mol%), and. [f] $Pd(OAc)_2$ (2 mol%). [g] Yields are reported as the HPLC yield from the reaction mixture. [h] Ag_2CO_3 (0.36 mmol). [i] Isolated yield by column chromatography.

a mixture of Ag(OAc) (3.0 eqv., 0.54 mmol) and sodium salt of TFA (2.0 eqv., 0.36 mmol) were tested both in acetic acid (Table 1, entries 12 and 18) and dioxane (Table 1, entry 13) as a solvent. To our dissatisfaction, none of these was as good as Ag_2O (Table 1, entries 12–13 *vs.* 3). Reducing the silver oxide stoichiometry (1.5 eqv., 0.27 mmol and 1.0 eqv., 0.18 mmol) was not shown to decrease the product yield significantly; however, 2.0 eqv. (0.36 mmol) of Ag_2O was considered to be the optimized additive loading. The catalyst loading was also monitored. Reducing $Pd(OAc)_2$ from 10 mol% (Table 1, entry 3) to 5 mol% (Table 1, entry 16) and further to 2 mol% (Table 1, entry 17) dramatically compromised the reaction yield. Finally, we found that the use of 10 mol% of $Pd(OAc)_2$ as a catalyst, in combination with 2.0 eqv. (0.36 mmol) of Ag_2O and 2.0 eqv. of iodobenzene, in the reaction of amide **3a** in acetic acid (as the solvent), at 120 °C for 10 h produced the corresponding C2-arylated product **4a1** in 86% isolated yield, with a high selectivity. Under the optimized condition, to explore the substrate scope, 1-naphthamide **3a** was primarily subjected to selective coupling with various aryl/heteroaryl/cycloalkyl halides. The investigation encompassed aryl iodides, aryl bromides, 2-iodo-pyridine, 4-iodo-pyridine, 5-iodo-1*H*-indole and 5-iodo-1*H*-imidazole, cyclopentyl bromide, and cyclohexyl bromide. The results demonstrated that only aryl iodides successfully afforded the desired products, while cycloalkyl bromides remained unreactive. With different heterocyclic iodides, we observed that the starting material **3a** majorly remained unconsumed, with a very trace non-isolable new product formation observed, as determined by the HPLC analysis of the crude reaction mixture after 10 h (SI, Table S1). The poor product conversion observed with nitrogen-containing heterocyclic iodides is presumably because of the ring nitrogen coordination with palladium, which might restrict further reaction. To gain further insight into the aryl iodide versatility, we examined various aryl iodides bearing electron-donating groups (EDG) and electron-withdrawing groups (EWG) at different positions for the regioselective C2–H arylation of 1-naphthamide. Both electron-deficient and electron-

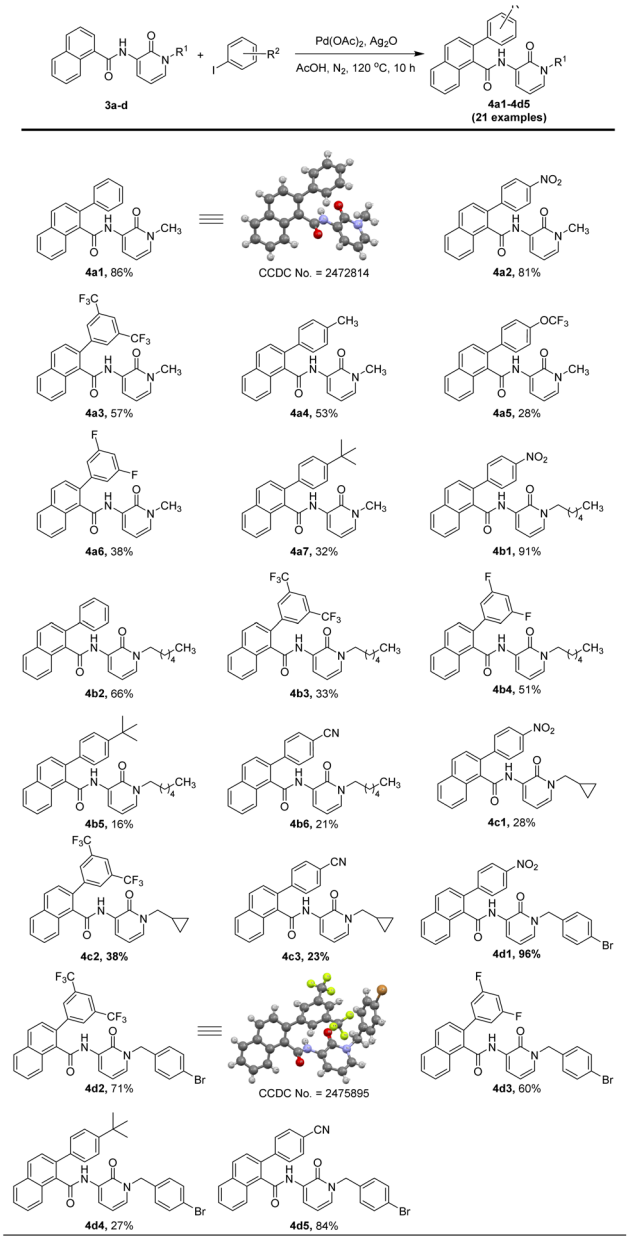

Scheme 3 Substrate scope for the 2-pyridone-assisted C2–H arylation of 1-naphthamides.

 © 2026 The Author(s). Published by the Royal Society of Chemistry

Open Access Article. Published on 03 March 2026. Downloaded on 3/16/2026 10:14:35 PM.
This article is licensed under a Creative Commons Attribution-NonCommercial 3.0 Unported Licence.

rich aryl iodides proved compatible with the reaction conditions, delivering the corresponding regioselective C2-arylated products **4a1–4d5** in good yields (Scheme 3). Different *N*-protected 2-pyridones served equally well (Scheme 3), offering a broader scope for structural modality. To identify the reasons for the few low yields, such as for products **4b5** (16%), **3b6** (21%) and **4c3** (23%), we performed HPLC analysis on the crude reaction mixture after 10 h and compared the HPLC retention time with that for the isolated standard sample. In all three reactions, we observed the complete consumption of both the reactants and the formation of undesired by-products, which lowered the yield of these products. The chromatography results are summarized in SI (Table S2). We further investigated whether our optimized reaction protocol was also successful in the 2-pyridone-directed 2-naphthamide system. *N*-(1-methyl-2-pyridone)-2-naphthamide (**3e**) was subjected to C–H arylation with iodobenzene under an identical reaction condition (Scheme 4). To our satisfaction, the method confirmed the formation of a C3-selective arylated product *N*-(1-methyl-2-pyridone)-3-phenyl-2-naphthamide (4×10^1) in 84% isolated yield (Scheme 5). To validate that the catalytic pathway proceeds through five-membered palladacycles, we protected the amide nitrogen of *N*-(1-methyl-2-pyridone)-1-naphthamide (**3a**) with a methyl group to prepare *N*-methyl-(1-methyl-2-pyridone)-1-naphthamide (**3f**). When **3f** was chosen as a substrate, as expected, no arylated product was observed even after 20 h, under an identical reaction condition (Scheme 5). This finding confirms the essential role of the free amide nitrogen in facilitating the transformation through coordination-assisted metalation.

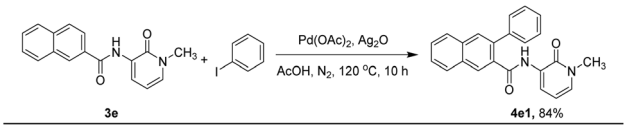

Scheme 4 2-Pyridone directed C–H arylation of 2-naphthamide.

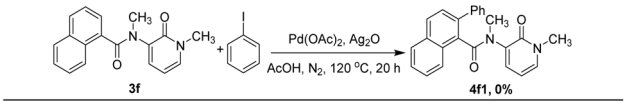

Scheme 5 2-Pyridone assisted C2–H arylation of *N*-methyl substituted 1-naphthamide.

The presence of Ag_2O is important, as it regenerates the Pd catalyst, generating by-products like AgI, H_2O, and Ag in the cycle. Also, the directing group, 2-pyridone, helps in providing stability by forming a bidentate complex with the Pd(II) intermediate. On the basis of the known Pd-catalyzed cycle[13] and DFT calculation (Fig. 2), we proposed a plausible $Pd(OAc)_2$-catalyzed regioselective reaction mechanism for the reaction of **3a** with iodobenzene to give **4a1** as the product. The first step involved the coordination of **3a** with Pd(II), followed by the formation of the active catalyst complex of Pd(II) **INT-1** *via* **TS-1**, with the elimination of AcOH (Scheme 6).

Further, **INT-1** undergoes C–H activation at the C2 position in 1-naphthamide through **TS-2** to yield **INT-2**, accompanied by the elimination of AcOH. In the next step, **INT-2** undergoes the oxidative addition of iodobenzene through **TS-3** to generate **INT-3**, where the Pd acquires an oxidation state of +4. The addition of AcOH afforded **INT-4** *via* **TS-4**, with the highest energy barrier of 14.14 kcal mol^{-1}. This step is the rate-determining step of the reaction. During the reductive

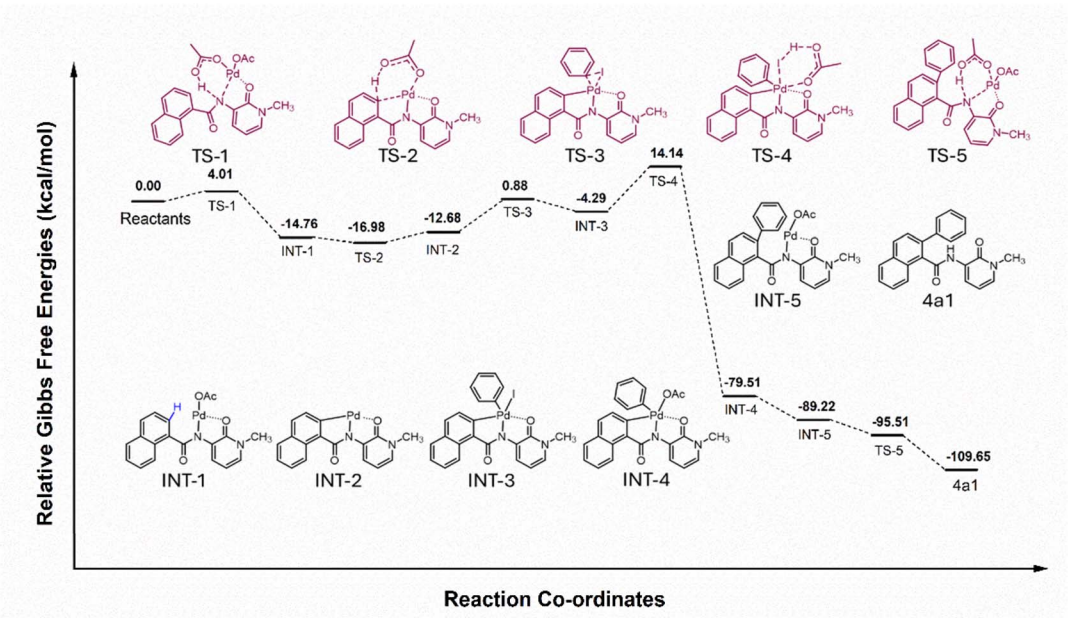

Fig. 2 Predicted mechanistic pathway and free-energy variation (in kcal mol^{-1}). Calculation was carried out at the B3LYP def2-TZVP, SMD(CH_3COOH) level of theory.

Open Access Article. Published on 03 March 2026. Downloaded on 3/16/2026 10:14:35 PM.
This article is licensed under a Creative Commons Attribution-NonCommercial 3.0 Unported Licence.

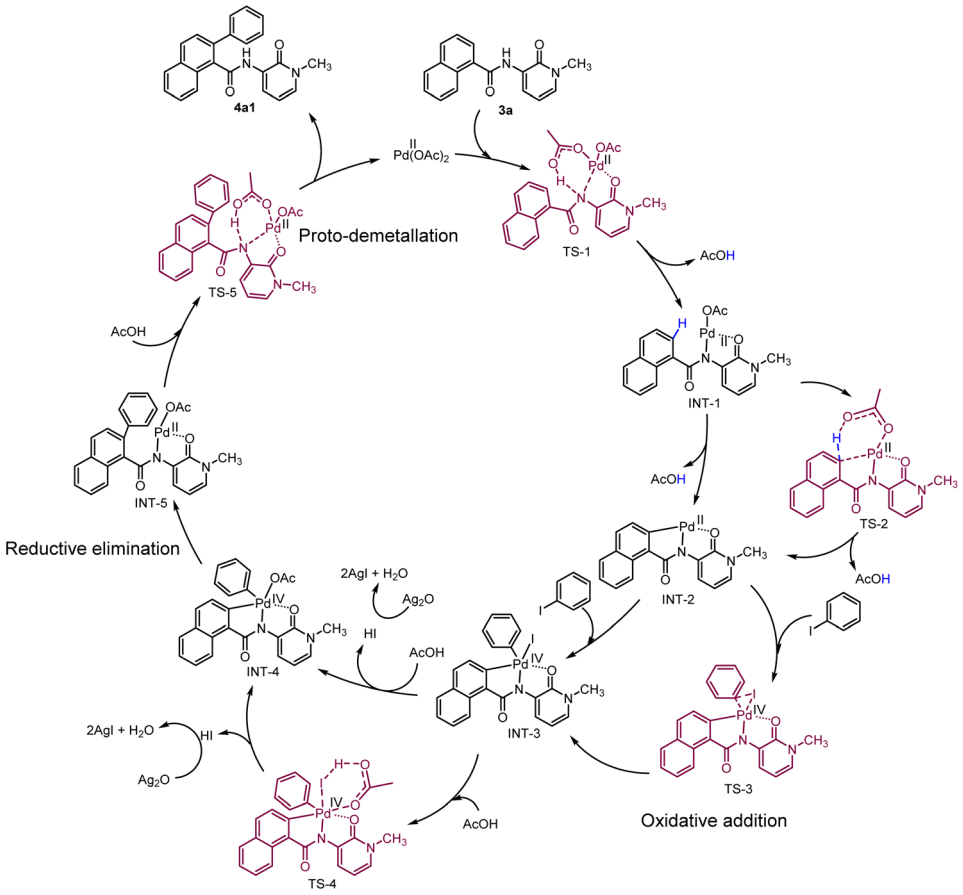

Scheme 6 Plausible catalytic cycle.

elimination, the Pd(II)-metal complex gives the C2-arylated 1-naphthamide (**INT-5**), followed by proto-demetallation through **TS-5** to afford the arylated product **4a1**. *In situ* Pd(II) undergoes catalyst regeneration for the next catalytic cycle using Ag_2O as the oxidant and AcOH as the solvent, with the formation of AgI, H_2O, and Ag as side products (Scheme 6).

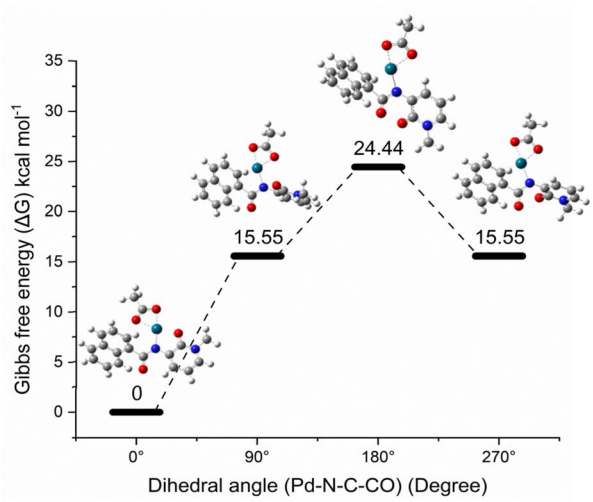

Fig. 3 Solvent-corrected relative Gibbs free energy profile for palladium intermediate complex at different dihedral angle (Pd–N–C–CO) 0°, 90°,180°, and 270°. Calculation was carried out at the RHF def2-SVP, SMD(CH_3COOH) level of theory.

To validate the role of 2-pyridone in the catalytic cycle, we extended our study to understand the stability of palladium intermediate complex at deferent dihedral angles (Pd–N–C–CO) of 0°, 90°, 180°, and 270°. We conducted computational calculation using Orca at the RHF def2-SVP, SMD(CH_3COOH) level of theory. With a constraint dihedral angle, all geometry were optimized at the same level of theory. The relative energy suggests that the intermediate with a dihedral angle of 0° has the lowest Gibbs free energy. With increasing the dihedral angle, the energy value increases; for example, 90° and 180° dihedral angles give 15.55 kcal mol^{-1} and 24.44 kcal mol^{-1}, respectively. To our expectation, when Pd comes in proximity to the carbonyl group of 2-pyridone, the energy goes down to 15.55 kcal mol^{-1} (Fig. 3). The results highlight that 2-pyridone assists in the catalytic cycle by stabilizing the palladium center *via* a five-membered palladacycle intermediate.

Conclusions

In conclusion, we demonstrated that 2-pyridone, a fundamental building block in medicinal chemistry, could be used as a bidentate directing group for the palladium-catalyzed

 © 2026 The Author(s). Published by the Royal Society of Chemistry

Open Access Article. Published on 03 March 2026. Downloaded on 3/16/2026 10:14:35 PM. This article is licensed under a Creative Commons Attribution-NonCommercial 3.0 Unported Licence.

regioselective C2(sp^2)–H arylation of 1-naphthamides. Our wide structural diversification also extended to showcase that 2-naphthamides can equally offer regioselective C3(sp^2)–H arylated products. The advantageous use of the ligand-free reaction condition and the formation of non-toxic byproducts, such as H_2O and Ag, highlight more possibilities for structural diversification in medicinal chemistry.

Author contributions

All authors have given approval to the final version of the manuscript.

Conflicts of interest

There are no conflicts to declare.

Data availability

Crystallographic data for **4a1**, **4d2** has been deposited at the CCDC under number: 2472814 and 2475895.[14a,b]

The data supporting this article have been included as part of the supplementary information (SI). Supplementary information is available. See DOI: https://doi.org/10.1039/d6ra00358c.

Acknowledgements

SC and JP acknowledge the financial aid provided by Axis Bank to support this research work. SC and JP also acknowledge Ashoka University for providing research infrastructure. JP thanks Ashoka University for funding support in terms of a Research Scholarship. The authors gratefully acknowledge the high-performance computing facility provided by Ashoka University.

References

1 S. Lin, C. Liu, X. Zhao, X. Han, X. Li, Y. Ye and Z. Li, *Front. Chem.*, 2022, **10**, 869860.
2 M. A. Ahmed, S. I. Alqasoumi, A. E. Ashour, V. Masand, N. A. Al-Jaber, B. H. Taibi and M. A. Mohamed, *Eur. J. Med. Chem.*, 2012, **53**, 133–140.
3 K. S. Kim, L. Zhang, R. Schmidt, Z.-W. Cai, D. Wei, D. K. Williams, L. J. Lombardo, G. L. Trainor, D. Xie, Y. Zhang, A. Yongmi, J. S. Sack, J. S. Tokarski, C. Darienzo, A. Kamath, P. Marathe, Y. Zhang, J. Lippy, J. Sr. Robert, W. Barri, H. Benjamin, J. Gullo-Brown, V. Manne, J. T. Hunt, J. Fargnoli and R. M. Borzilleri, *J. Med. Chem.*, 2008, **51**(17), 5330–5341.
4 Z. Liu, Y. Yuan, M. Kogiso, B. Zheng, L. Deng, J. J. Qiu, S. Dong, H. Lv, J. M. Gallo, X.-N. Li and Y. Song, *J. Med. Chem.*, 2014, **57**(20), 8307–8318.
5 F. Wu, H. Jiang, B. Zheng, M. Kogiso, Y. Yuan, C. Zhou, X.-N. Li and Y. Song, *J. Med. Chem.*, 2015, **58**(17), 6899–6908.
6 K. Kusakabe, Y. Tada, Y. Iso, M. Sakagami, Y. Morioka, N. Chomei, S. Shinonome, K. Kawamoto, H. Takenaka, K. Yasui, H. Hamana and K. Hanasaki, *Bioorg. Med. Chem.*, 2013, **21**(7), 2045–2055.
7 P. S. Dragovich, T. J. Prins, Ru Zhou, E. L. Brown, F. C. Maldonado, S. A. Fuhrman, L. S. Zalman, T. Tuntland, C. A. Lee, A. K. Patick, D. A. Matthews, T. F. Hendrickson, M. B. Kosa, Bo Liu, M. R. Batugo, J.-P. R. Gleeson, S. K. Sakata, L. Chen, M. C. Guzman, J. W. Meador, A. F. Rose and S. T. Worland, *J. Med. Chem.*, 2002, **45**(8), 1607–1623.
8 J. W. Skiles, R. Sorcek, S. Jacober, C. Miao, P. W. Mui, D. McNeil and A. S. Rosenthal, *Bioorg. Med. Chem. Lett.*, 1993, **3**(4), 773–778.
9 L. Ningning, C. Zhengkai, L. Yue, L. Zhanxiang and Z. Yuhong, *Org. Lett.*, 2018, **20**(18), 5845–5848.
10 S. L. Yedage and B. M. Bhanage, *J. Org. Chem.*, 2016, **81**(10), 4103–4111.
11 P. Li, G.-W. Wang, H. Chen and L. Wang, *Org. Biomol. Chem.*, 2018, **16**, 8783–8790.
12 (*a*) T. K. Pati, S. Debnath, M. Kundu, U. Khamrai and D. K. Maiti, *Org. Lett.*, 2018, **20**(13), 4062–4066; (*b*) T. K. Pati, S. Ali Molla, N. N. Ghosh, M. Kundu, S. Ajarul, P. Maity, U. Khamrai and D. K. Maiti, *J. Org. Chem.*, 2024, **89**(10), 6798–6812.
13 V. G. Zaitsev, D. Shabashov and O. Daugulis, *J. Am. Chem. Soc.*, 2005, **127**(38), 13154–13155.
14 (*a*) CCDC 2472814: Experimental Crystal Structure Determination, 2026, DOI: 10.5517/ccdc.csd.cc2p0563; (*b*) CCDC 2475895: Experimental Crystal Structure Determination, 2026, DOI: 10.5517/ccdc.csd.cc2p3cls.